Colloidal iron and organic carbon control soil aggregate formation and stability in arable Luvisols

Lars Krause[a,b], Erwin Klumpp[a], Ines Nofz[a], Anna Missong[a], Wulf Amelung[a], Nina Siebers[a]

[a] Institute of Bio- and Geosciences, Agrosphere (IBG-3), Forschungszentrum Jülich GmbH, Wilhelm Johnen Straße, 52425 Jülich, Germany

[b] Institute for Environmental Research, Biology 5, RWTH Aachen University, Worringerweg 1, 52074 Aachen, Germany

Keywords: microaggregates, field flow fractionation, wetting-drying, size distribution, disaggregation, aggregation

Correspondence: Dr. Nina Siebers, Institute of Bio- and Geosciences, Agrosphere (IBG-3), Forschungszentrum Jülich GmbH, Wilhelm Johnen Straße, 52425 Jülich, Germany, Phone: +49-2461-61-96614, n.siebers@fz-juelich.de

Abstract

Several beneficial soil functions are linked to aggregates, but how the formation and stability depend on the presence of colloidal- and nanosized (1000-1 nm) bulding blocks is still understood poorly. Here, we sampled subsites from an arable toposequence with 190 and 340 g kg^{-1} clay, and isolated small soil microaggregates (SMA; < 20 µm) from larger macroaggregate units (> 250 µm) using an ultrasonic dispersion energy of 60, 250, and 440 J mL^{-1}, respectively. We then allowed these small SMA to reaggregated after chemical removal of organic carbon (OC) as well as of Fe- and Al (hydr)oxides, respectively. The size distribution of the reaggregated small SMA and fine colloids (< 0.45 µm) was analyzed via laser diffraction and asymmetric flow field-flow fractionation coupled to inductively coupled plasma mass spectrometry and organic carbon detection, respectively. We found elevated amounts of both finer colloids and stable SMA at subsites with larger clay contents. The size distribution of small SMA was composed of two distinctive fractions including colloids and larger microaggregates with an average size of 5 µm. The removal of Fe with Dithionite-Citrate-Bicarbonate (DCB) shifted the size of the small SMA to a larger equivalent diameter, while removal of OC with NaOCl reduced it. After three wetting and drying cycles, the concentration of colloids declined, whereas the small SMA without chemical pre-treatments reaggregated to particles with larger average diameters up to 10 µm, with the size depending on the clay content. Intriguingly, this gain in size was more pronounced after Fe removal, but it was not affected by OC removal. We suggest that Fe (hydr)oxides impacts the stability of small SMA primarily by being present in small-sized pores and thus cementing the aggregates to smaller size. In contrast, the effect of OC was restricted to the size of colloids, gluing them together to small SMAs within defined size ranges when OC was present but releasing these colloids when OC was absent.

1. Introduction

Physical and ecological soil functions such as storage and stabilization of OC, the allocation of microbial habitats or the water holding capacity are coupled to the architecture and composition of soil aggregates. Intensive land use or land use changes induce dynamic changes in the soil structure (e.g., Bronick and Lal, 2005; Siebers et al., 2018a, Siebers and Kruse, 2019). In order to predict these changes, it is necessary to quantify the soil aggregates and their properties including aggregate stabilizing components. Especially the smallest structures in the size range of colloids (1000 to 100 nm) have the potential to contribute to the different aggregate hierarchy levels since they can either be highly mobile or reactive depending on different environmental variables.

To better understand the mechanisms of aggregate formation and stabilization, soil aggregates have been conceptualized into hierarchical orders, with macroaggregates (> 250 µm) being composed of large (250-20 µm) and small (20-2 µm) soil microaggregates (SMA) (Christensen, 1996; Oades and Waters, 1991; Tisdall and Oades, 1982), as well as of clay- and silt-sized organo-mineral associations also called composite building units (< 2 µm) (Totsche et al., 2018). Further efforts differentiated between free and occluded SMA and thus between SMAs occurring within or outside larger macroaggregate associations (Six et al., 2004; Six et al., 2002).

The size range of the composite building units (< 2 µm) also contains the so-called soil colloids (1000-450 nm), fine colloids (450-100 nm) and nanoparticles (100-1 nm) (Christian et al., 2008; Gottselig et al., 2017). The composition of soil colloids is a function of the mineralogical composition of the soil clay fraction (Kretzschmar, 2005). The colloids and nanoparticles comprise inorganic or organic particles or both, e.g., clay minerals, metal (hydr)oxides (oxides, hydroxides, and oxyhydroxides), and humic substances. Especially Fe (hydr)oxides are known to play a crucial role for stabilizing soil microaggregates, as the Fe speciation influences microaggregate structure and stability. The Fe may be present as free Fe-(hydr)oxide nanoparticles being as small as 2 to 5 nm, as Fe-(hydr)oxides associated with clay minerals, and as Fe in clay minerals (Regelink et al., 2014). On the one hand, colloidal Fe-(hydr)oxides are important building units of the aggregate system actively promoting the formation and stabilization of soil aggregates (Schwertmann, 2005, Totsche et al., 2018). On the other hand, under anaerobic conditions, e.g., in water-saturated soils or

enclosed within soil aggregates, Fe(III) can be used by specialized microorganisms as an alternate electron acceptor leading to the formation of Fe(II) compounds being highly soluble. This in turn leads to a destabilization of aggregates when Fe is integrated as cementing agent. When in contact with oxygen again, dissolved Fe(II) is reprecipitated to Fe-(hydr)oxides. Thus, the dynamic weathering reactions of Fe to a great extent also determine many aspects of soil aggregation and stability. With decreasing diameter of the aggregates, their stability generally increases (Golchin et al., 1994; Tisdall, 1996) and the turnover of associated elements decrease (Siebers et al., 2018b). While different parts of organic matter have been found to be responsible for differences in the stability of micro- and macroaggregates (Caravaca et al., 2004; Haynes and Swift, 1990; Ladd et al., 1993; Tisdall and Oades, 1982; Totsche et al., 2018), the stabilizing interactions within the class of SMAs is less clear. Totsche et al. (2018) hypothesized that especially composite building units (< 2 µm) control microaggregation across the different size levels, but particular mineral and organic fine colloids (< 0.45 µm) and nanoparticles (< 0.1 µm) are of importance as potential building blocks and stabilizing agents of the aggregate structure (Totsche et al., 2018).

Clay minerals may be involved in different aggregation mechanisms based on electrostatic forces; for example, plate-like clay minerals are able to homoaggregate and form a cardhouse structure with bivalent cations due to their different edge and face charges, whereas different geometry is likely reached in presence of monovalent cations (Weil and Brady, 2017). In addition, clay particles can directly form aggregates with other minerals (Denef and Six, 2005; Fernández-Ugalde et al., 2013), e.g., with positively charged Fe and Al (hydr)oxides (Ferreiro et al., 1995; Totsche et al., 2018). A recent study thus suggested the clay fraction to be the primary factor for the formation of clay mineral-oxide microaggregates, with the formed heteroaggregates being more stable than homoaggregates (Dultz et al., 2019). The formed composite units (include different building units, e.g., clay minerals and Fe (hydr)oxides) can be described as secondary particles and are usually stabilized by organic matter (OM) as gluing agent (Totsche et al., 2018). This OM may both be adsorbed on the mineral surfaces (Guggenberger and Kaiser, 2003; Lehmann et al., 2007; Wagai and Mayer, 2007) or encapsulated in-between minerals (Chenu and Plante, 2006; Snyder and Vázquez, 2005). These processes are not exclusive but likely occur simultaneously. Disentangling these various interactions in SMA formation and stabilization is difficult and can hardly deduced from mere characterization of SMA properties. However, it is possible to disrupt SMAs at certain

energy levels, and then to allow them to reaggregate (Siebers et al., 2018a), a process, which we can manipulate by sequential removal of cementing or gluing agents. Re-aggregation, in turn, may be accelerated by repeated wetting and drying (Denef et al., 2001; Kaiser et al., 2015; Utomo and Dexter, 1982).

Here, we hypothesized that reaggregation of SMAs is only achieved in the presence of both colloidal- and nanosized Fe (hydr)oxides and OC. To test this hypothesis, we subjected the macroaggregates of a Luvisol of different clay content to mechanical (ultrasound) and chemical (removal of Fe-oxides and removal of OC) disintegration and analyzed the reaggregation potential of the released microaggregates after three wetting-drying cycles. Thereby we evaluated the chemical composition and size distribution of small SMA and the fine colloid fraction.

2. Material and methods

2.1 Sampling

Arable Luvisols were sampled along a toposequence within the same plot at the German research station in Scheyern (48° 29´ 36´´ N, 11° 26´ 15´´ E), which was characterized by a sandy to loamy texture. As the upper Ap layer showed evidence of crust formation, we removed the top 4-5 cm of soil before samples were taken with an auger (16 cm diameter, 15 cm depth). We selected these sampling sites since they had the same management but the sampling points differed in clay contents, and they were also free of carbonates; thus, the soils exhibited excellent conditions in order to answer our research questions. The soil was mainly composed of illitic clay minerals (Krause et al., 2018) and of low- to- moderate smectite and vermiculite contents, which did not show systematic differences across the texture gradient (K. U. Totsche, K. Eusterhues, P. Ivanov, personal communication, 2018). Other clay minerals detected were Fe-chlorite, kaolinite and smectite. For this study, we analyzed the soil with the smallest (19%) and largest (34%) clay content (Table 1) in triplicates. The field fresh samples went through an experimental procedure including the isolation of occluded small SMA, removal of Fe and OC, reaggregation (Fig. 1), and subsequent chemical analyses as described in the following sections.

2.2 Fractionation

The wet-fractionation and differentiation between free and occluded SMA was performed analogously to Krause et al. (2018). The SMA mass distribution of free and occluded SMA for small and large clay content can be found in Krause et al. (2018). Generally, the main differences between samples with small and large clay content were the amount of occluded small SMA, the proportion of which was significantly higher in soils with large clay content (Krause et al., 2018). Overall, 60 g of field-moist samples were pre-wetted in H_2O for 5 min, followed by wet-sieving. The macroaggregate fraction (> 250 µm) was collected on the sieve and the free SMA fraction (< 250 µm) was discarded. In order to release occluded SMA at different stability levels, collected macroaggregates were subjected to separate ultrasonic treatments (Digital Sonifier 450, Branson Ultrasonics corp., Connecticut, USA) with an energy of 60, 250, and 440 J mL^{-1}, respectively. The occluded SMA fraction released from macroaggregates was wet-sieved to collect the small SMA fraction (< 20 µm). The small SMA suspension was centrifuged using 7270 x g for 85 min to collect the solid phase.

Primary sand and silt particles were removed from small SMA in sodium metatungstate (SMT) solution referring to Virto et al. (2008) at a density of 2.5 g cm^{-3} using centrifugation with 19320 x g for 50 min. The < 2.5 g cm^{-3} fraction containing SMA was collected in a vessel by pipetting. Since the < 2.5 g cm^{-3} fraction could not be collected in one step, the density fractionation was repeated three times by resuspension of the remnants in SMT and centrifugation. The < 2.5 g cm^{-3} fraction was washed three times, each in 130 mL H_2O, followed by the separation of the solid from the aqueous phase by pipetting after centrifugation at 7270 x g for 85 min. For the investigated soils the mass percentage of the < 2.5 g cm^{-3} fraction was 69% (small clay content, 19% clay) and 56% (large clay content, 34% clay), respectively. As the samples contained little if any particulate organic matter residues (Krause et al., 2018), we considered this < 2.5 g cm^{-3} fraction as being largely SMA without additional primary mineral particles such as sand.

2.3 Removal of Fe and OC

Poorly crystalline and crystalline Fe (hydr)oxides were removed from the fractionated small SMA using the Dithionite-Citrate-Bicarbonate (DCB) method developed by Mehra and Jackson (1958), mainly extracting Fe oxyhydroxides and partially Mn, Al, and Si (Bigham et al., 1978; Kiem and Kögel-Knabner, 2002). Note that the DCB treatment did not remove Fe completely (Borggaard, 1988; Varadachari et al., 2006).

Especially small sized particles may be removed, as DCB is generally known to dissolve pedogenic Fe-oxide (e.g., hematite or goethite) by reduction. The size range of hematite or goethite is between 0.02 to 0.1 µm (Tan et al., 2006); therefore, partial loss of nanoparticles and colloids were expected and reasonable. The Fe extraction with DCB was repeated once and the samples were washed three times, each in 30 mL H_2O and centrifuged with 14500 x g for 35 min and the supernatant was discarded. The gained pellets were resuspended in 25 mL H_2O for further analysis.

Sodium hypochlorite (NaOCl) was selected for the OC removal, since it preserves widely the mineral phase (Mikutta et al., 2005). Nevertheless, the NaOCl does not completely remove OC from the sample since poorly crystalline minerals can protect to some extent the OC against the oxidative destruction (Kaiser and Guggenberger, 2007; Mikutta et al., 2005). The OC was removed from small SMA in 6% NaOCl at a pH of 8.5 under continuous stirring. The sample was incubated in NaOCl for 3 h, followed by centrifugation at 14500 x g for 15 min and discarding the supernatant. The pellet was resuspended in NaOCl and stirred for 16 h. After the NaOCl was removed from the sample by centrifugation at 14500 x g for 15 min, the sample was washed in 1 M NaCl, centrifuged at 14500 x g for 35 min, followed by two washing steps covering resuspension of the pellet in H_2O, centrifugation at 14500 x g for 35 min, and discarding the supernatant. The gained pellets were resuspended in 25 mL H_2O for further analysis.

In order to control the performance of the chemical treatments, freeze-dried aliquots were ground and digested with aqua regia (50 mg sample in 2.7 mL) in the microwave. After digestion the aliquots were analyzed with inductively coupled plasma (ICP) optical emission spectrometry (OES) in a 1:20 (v:v) dilution.

2.4 Reaggregation experiment

Repeated wetting and drying was used to initiate the reaggregation of small SMA. For the reaggregation only the small SMA that were released by ultrasonication with 440 J mL^{-1} were investigated. Non-treated small SMA (served as control) and those with removed Fe and OC were subjected to three repeated wetting (for 24 h) and drying cycles. The wetting and drying was executed on 10 mL of small SMA suspensions with an average electrical conductivity of 5 µS cm^{-1} and a pH of 5.6 at room temperature in glass petri dishes. Complete air-drying of the samples was monitored via the weight-loss. Thereafter, the evaporated volume

was replaced with H_2O with a pipette to allow the particles to resuspend for the wetting phase. After three completed wetting and drying cycles the small SMA were resuspended in 20 mL H_2O for further analysis.

2.5 Size distribution

Size distribution images were compiled from micrographs measured by a microparticle detector (PN3000 XPT, Postnova Analytics GmbH, Landsberg am Lech, Germany) combined with the image analysis software ImageJ (v.1.52d, National Institutes of Health, Bethesda, USA). Color coded images were generated by overlaying 250 recorded single images, which went through an image processing pipeline including 8-bit conversion, background subtraction, particle analysis, color coding, and overlapping of all overlay images. In the finalized figures, all detected aggregates are shown in different colors in dependence of their two-dimensional surface area.

The volume-based particle-size distribution in suspensions was analyzed via laser diffraction (LA-950, Horiba, Kyōto, Japan). With the internal ultrasonic finger of the laser particle-size analyzer the samples were sonicated before each measurement using 13 J mL^{-1}. Under continuous stirring the samples were measured in a flow-through cell where light in two wavelengths was applied (650 and 405 nm). The data about scattering angle and light intensity was measured by the detectors and transformed by a software algorithm into a volume-based size distribution using the Mie-theory (Eshel et al., 2004) provided by the manufacturers' software. For comparison, the size distributions were overlapped and the overlapping area for each replicate was determined in percent in Origin (OriginPro 2018b, Originlab, Massachusetts, USA) for further statistical analyses.

2.6 FFF-UV-OCD-ICP-MS

Fine colloids (< 0.45 µm) were separated and analyzed the < 0.45 µm fraction via AF4 coupled to ICP mass spectrometry (MS) and OCD (Gottselig et al., 2017; Jiang et al., 2015; Missong et al., 2018) in order to receive the elemental concentration of fine colloids over the whole distribution. Before analysis with FFF the sample suspensions were filtered through a 0.45 µm PVDF filter (P667.1, Rotilabo, Carl Roth GmbH & Co. KG, Karlsruhe, Germany) and diluted 1:5 (v/v) with H_2O. Fine colloids were fractionated via asymmetric flow field flow fractionation (AF4) (AF2000, Postnova analytics, Landsberg am Lech, Germany) and analyzed

208 online with a coupled OC detector (OCD; LC-OCD Model 8, DOC-Labor Dr. Huber, Karlsruhe, Germany)
209 and an ICP- mass spectrometer (MS) (ICP-MS; Agilent 7500, Agilent Technologies, Santa Clara, USA).

210 The separation channel of the AF4 was equipped with a 500 µm spacer and a 1 kDa PES membrane. A
211 concentration of 25 µM NaCl carrier solution was used. Overall 2 mL of sample was injected to the
212 fractionation channel using a flow rate 0.2 mL min^{-1}. The fine colloids were focused for 20 min using a focus
213 flow of 3.3 mL min^{-1} and a cross flow of 3 mL min^{-1}. After a transition time of 1 minute the focus flow was
214 switched off and the cross-flow rate was kept constant for 15 min. The fine colloids were stepwise eluted
215 from the channel with 0.5 ml min^{-1} by reducing the crossflow exponentially from three to zero mL min^{-1} using
216 the power mode. The 0.06-0.45 µm fraction contained particles of the “release-peak”, once the cross-flow
217 was switched off. At this point these particles are not perfectly separated by their size (described by
218 Neubauer et al. (2013)) and therefore indicated with the letter “R” in the corresponding fractograms.

219 After the samples eluted from the channel according to their size and physicochemical properties, they were
220 analyzed by the detectors. In order to characterize the elution timeframes for different size classes, the
221 method was validated by fractionation of latex standards (0.06, 0.22, and 0.02 µm) before the
222 measurements. The elution profile was evaluated with the UV-vis detector measuring the relative absorption
223 of UV (254 nm) by the eluted sample over time. The elemental composition of eluted fine colloids was
224 analyzed online with ICP-MS and the quantification of was carried out by an external multipoint calibration
225 and linear regression. The OC was measured by the OCD detector and quantified by an internal multipoint
226 calibration and linear regression. Baseline correction, data analyses and integration for element
227 quantification was performed in Microsoft Excel (Microsoft Excel 2010, Microsoft Corporation, Washington,
228 USA) and OriginLab (OriginPro 2017, OriginLab, Massachusetts, USA).

229 ## 2.7 Statistical analyses

230 Statistical analyses were performed in Excel (Excel 2010, Microsoft Corporation, Washington, USA) and
231 Origin (OriginPro 2018b, Originlab, Massachusetts, USA). The normal distribution was tested using the
232 Kolmogorow-Smirnow-Test test and variance homogeneity was evaluated by Levene’s test.

233 Differences in the isolated SMA mass were evaluated statistically according three factors (clay content,
234 ultrasonic energy and chemical treatment) with a three-way ANOVA comparing whether population means

originate from the same distribution at a significance level of α= 0.05. After that, a post-hoc analysis was performed using the Bonferroni test for the identification of significant differences between the compared groups including their interaction. Changes in the elemental composition after the application of different chemical treatments were evaluated for each element and clay content separately with a one-way ANOVA comparing whether population means originate from the same distribution at a significance level of α= 0.05. Differences between the compared groups were identified with a post-hoc analysis using the Bonferroni test.

Size distributions were compared by the percentage of their overlapping area, which was evaluated statistically with a two-tailed t-test at a significance level of α= 0.05. Four levels of significance were defined and are indicated by asterisks (not significant, p> 0.05, no symbol; significant, p≤0.05, *; very significant, p≤0.01, **; highly significant, p≤0.001, ***; extremely significant, p≤0.0001, ****). The significance of increase or decrease of the individual elements in fine colloids after reaggregation was tested with a two-tailed t-test against the original mass before reaggregation.

3. Results

3.1 Mass and particle size distribution of small SMA

Occluded small SMA were released from the macroaggregate fraction at all three levels of ultrasonic energy (60, 250, and 440 J mL^{-1}). The yields of small SMA (Fig. 2) were larger for the sites with larger clay content (84-116 g occluded SMA kg^{-1} field fresh soil) than for the sites with 15% less clay (28-38 g occluded SMA kg^{-1}) but hardly different among dispersion levels, except for the site at larger clay content, at which significantly more small SMA were released from the macroaggregate fraction using 440 J mL^{-1} ultrasonic energy input than with the less energy input. In addition, treating the isolated SMA after fractionation with DCB or NaOCl for Fe and SOC removal reduced the SMA masses in average by 11%.

The size distribution of small SMA suspensions was analyzed using XPT microparticle detection and laser diffraction. Overlays of micrographs from the microparticle detector (see appendix Fig. A.1) revealed that the small SMA fraction was mainly composed of smaller units with a surface area of < 53 μm^2, referring to a wadell disk diameter (diameter of a circle having the same area of the measured particle/aggregate) of

8.2 µm. The remaining detected microaggregates reached areas of 315 μm^2, which referred to a diameter of 20 µm, the upper limit of small SMA.

Further comparison of size distributions were based on laser diffraction analysis since it enabled the analysis of particles down to 0.01 µm (Fig. 3). The size distribution of small SMA from soils with small (Fig. 3a-c) and large (Fig. 3d-f) clay content ranged between 0.06 and 20 µm showing a bi-modal pattern peaking in average sites at 0.24 and 4.7 µm. Peak integration revealed that, on average, 74% of the detected particles were > 1 µm.

At the subsites with 19% clay, the size distributions of the occluded SMA were similar for ultrasonic treatments using 60 and 250 J mL^{-1} energy input. However, the size distributions significantly changed when switching to the highest ultrasonic treatment (larger stability level) using 440 J mL^{-1} energy input. At this energy level, we observed elevated proportions of colloids < 1 µm at the expense of larger subfrations (> 1 µm) of the SMA. For the subsites with 34% clay, the application of both 250 and 440 J mL^{-1} significantly shifted the size pattern to elevated proportions of colloids, which again occurred at the expense of the proportions of larger-sized SMA fractions (Fig. 3).

In contrast to elevated inputs of ultrasonic energy, effects of the chemical treatments on the particle-size distribution of occluded SMA were more apparent. Intriguingly, the DCB treatment significantly shifted the size distribution to larger particle sizes, peaking, on average, at 0.31 and 6.3 µm. Consequently, the DCB treatment increased the abundance of small SMA > 1 µm, now representing on average 80% of all detected small SMA. A different finding was recorded for samples treated with NaOCl for OC removal: a portion of small SMA decayed, and only 58-63% of all detected small SMA were represented by the size of > 1 µm depending on the clay content and ultrasonic level. The average particle size declined, peaking at 0.36 µm for colloids < 1 µm, which were more abundant than in the untreated samples and at 4.2 µm for the remaining small SMA. Generally, shifts in the size distribution pattern after DCB and NaOCl treatment (Fig. 3) are a complex interplay between removal of elements, disintegration of existing structures, and formation of new structures.

Different ultrasonic treatments did not alter the elemental composition of the small SMA (data not shown). However, the chemical treatments changed the elemental composition in the small SMA for both clay

contents (Fig. 4). After DCB treatment 52 and 36% of the Fe were removed from both the samples with small and large clay content. The Al concentration did not change in the samples with less amounts of clay, but decreased significantly by 33% for the ones with larger clay content (Fig. 4). In addition, the DCB treatment reduced the contents of OC by 17 and 21% and that of total N by 21 and 25% relative to the untreated samples with small and large clay content, respectively. This also means, that the added citrate to the dithionite-bicarbonate complex was not adsorbed to any degree that might have affected the final OC content. A much stronger reduction of OC content was reached by the NaOCl treatment, which eliminated 77 and 72% of OC and 89 and 84% of N for the samples with small and large clay content, respectively. Intriguingly, also the concentrations of Al in the samples with 34% clay were reduced by this NaOCl treatment (Fig. 4).

3.2 Reaggregation of small SMA and fine colloids

After the small SMA passed through three wetting- and drying cycles, the size distribution was measured again in order to evaluate the level of reaggregation for soils with small (Fig. 5a-c) and large (Fig. 5d-f) clay content. In both the samples with small and large amounts of clay, reaggregation occurred, the average particle-size diameter increased and nanoparticles and colloids < 1 µm almost vanished. In the Control, SMA were detected in the size range of 1-80 µm for the soil with small clay content (Fig. 5a) and 0.1-20 µm for that with large clay content (Fig. 5d). This means that in the soil with smaller clay content, for instance, the average size range of the small SMA increased by about to 10 µm.

When the small SMA had been treated with DCB prior to exposing them to wet-dry cycles, again, reaggregation occurred and it was even larger than for the samples that still contained their original Fe amounts. The final sizes of the reaggregated small SMA were in the range of 1-400 µm for soils with small clay content (Fig. 5b) and between 0.2-100 µm for those with larger clay content (Fig. 5e). For both clay contents the new maxima increased by another 10.5 µm. When the small SMA had been treated with NaOCl in turn, we did not observe significant changes in their size distribution after three wetting and drying cycles, as illustrated by SMA size ranges between 0.08-20 µm for both clay contents (Fig. 5c,f).

The fine colloids (< 0.45 µm) of the small SMA were further fractionated by AF4 and analyzed by OCD (Fig. 6 a,b) and ICP-MS (Fig. 6 c-h). According to the elution time from the separation channel, three size-classes were defined, i.e., < 0.02, 0.02-0.06, and 0.06-0.45 µm. The smaller concentrations of Fe, Al, and Si were indicative of less inorganic fine colloids from the soil with smaller clay content (see appendix Fig. A.2 c,e,g) than from the soil with larger clay content (Fig. 6c,e,g). In the size range of 0.06-0.45 µm, colloids were mainly composed of Fe, Al, and Si. In the smaller size classes, the colloids were characterized by lower concentrations of all inorganic elements (Fig. 6c-h). The OC concentration revealed a contrary pattern (Fig. 6 a,b). For both clay contents, the highest concentrations of OC were found in the smaller sized, fine colloid fractions.

When the samples were chemically treated with DCB and NaOCl, the distribution of elements changed. This change was particularly pronounced for the samples with larger clay content: After partial removal of Fe and OC from the small SMA, the element concentrations increased for Fe, Al, and Si, which is indicative for the release of fine colloids from small SMA. The largest concentrations were always found in the 0.06-0.45 µm fraction in the samples where OC was removed (Fig. 6c,e,g). With the partial removal of Fe, the concentration of OC increased, while after the reduction of OC from the small SMA, the OC concentration of the fine colloids was similar to that of the control (Fig. 6 a). After reaggregation of the small SMA with three wet-dry cycles, the analysis of the sub-fractions of fine colloids revealed that total changes mainly occurred in the 0.06-0.45 µm fraction rather than in < 0.06 µm fraction (Fig. 6b,d,f,h, appendix Fig. A.3).

4. Discussion

The applied mechanical energy through ultrasonication effectively released occluded small SMA from the macroaggregate fraction (Fig. 2). The results indicated that the stability of occlusion was lower with smaller clay content, which is likely due to the smaller surface area for interactions between clay minerals, gluing, and cementing agents. Our data thus support the idea that i) the clay fraction is a critical precondition for the formation of small SMA structures that are able to form macroaggregates (Tisdall and Oades, 1982; Totsche et al., 2018) and ii) the formation and quantity of stable macroaggregates is, among others, controlled by the clay content.

According to the study of Lehtinen et al. (2014), the breakdown of macroaggregates already starts at 2 J mL^{-1}, but the disaggregation strongly depends on the analyzed soils. For Mollisols, which are at least of similar texture to the soils under study, Amelung and Zech (1999) had suggested that macroaggregate breakdown was complete at disruption energies of 60 J mL^{-1}. And indeed, we hardly gained more small SMA when using higher ultrasonic energies. We thus have to assume that elevated energies of 440 J mL^{-1} or more may also have affected the small SMA itself, with 800 J mL^{-1} being reported as a typical dispersion maximum (Kaiser et al., 2012). Nevertheless, the application of ultrasonic energy needs always to be considered regarding the soil type and mineralogy; the maximum dispersion energy for Andisols can be much larger (in the range of 5000 J mL-1) as reported by Asano and Wagai (2014). However, we did not observe a significant alteration of element composition of small SMA with different ultrasonic energy input, suggesting that specific reactions of possible stabilizing agents like OC and Fe species are more important for aggregate stability than the ratio of single elements. Furthermore, the size distribution of the small SMA may also contributed to the different stability levels as indicated by significant changes with the largest ultrasonic treatment.

In difference to Krause et al. (2018), we improved our laser diffraction analysis by the application of an a-priori density fractionation for small SMA in order to prevent masking effects of larger primary mineral particles, since their large volume reduced the detection sensitivity for < 1 µm sized particles which represented only < 0.3% of the total detected volume. The modified method increased the sensitivity for the < 1 µm size fraction by increasing their volume percentage up to 3%, which now allows a more detailed analysis compared to the own previous investigations. The occluded small SMA were composed of two distinctive size fractions, which can be categorized into colloidal-sized building units mainly occurring in the < 1 µm fraction and the remaining larger building units and the small SMA occurring in the > 1 µm fraction (Fig. 3). The destruction of the larger fraction by higher ultrasonic energy input resulted in the release of their building units (Fig. 3), suggesting that the concept of aggregate hierarchy (Oades and Waters, 1991; Six et al., 2002; Tisdall and Oades, 1982) can be extended to the size range of small SMA, which was obviously largely composed of colloidal-sized building units (100-1000 nm). Within this size range, AF4-ICP-MS (Fig. 6) revealed another characteristic pattern, in which the size fraction < 0.06 µm was mainly composed of OC and the size fraction of 0.06-0.45 µm was mainly composed of inorganic components

(elements like Al, Si, and Fe). These compounds can be clay minerals, Fe, and Al (hydr)oxides that are found in soils as silicate-oxide associations rather than in their pure form (Churchman 2018).

The significant reduction of the contents of Fe, Al, and OC after DCB and NaOCl treatments in the small SMA (Fig. 4) was in line with previous studies on this topic (Bigham et al., 1978; Eusterhues et al., 2005; Kiem and Kögel-Knabner, 2002; Sowers et al., 2018; Zhao et al., 2016). Surface adsorbed OC was likely also removed with adjacent Fe-oxides (Eusterhues et al., 2005; Sowers et al., 2018; Zhao et al., 2016). For Fe-removal DCB was used, generally known to dissolve pedogenic Fe-oxide by reduction, whereas Al-oxides are largely insoluble in DCB. The removal of Al by DCB treatment is more difficult to explain because it should be independent from redox treatments. We thus speculate that the DCB-soluble Al predominantly likely represents the Al replacement in crystalline Fe minerals rather than Al in highly crystalline minerals such as gibbsite. Aluminum substitution in goethites, for instance, is well-known and can reach up to 33 mol% (e.g., Fitzpatrick and Schwertmann 1982). In addition, the removed Al may also include Al in non-crystalline Fe oxides as well as organically bound Al (Darke and Walbridge, 1994). The present citrate likely also contributed to the removal of the Al in the DCB treatment (Bigham et al., 1978; Kiem and Kögel-Knabner, 2002), The differences in Al concentrations for the 19% and the 34% clay content is thus probably mainly a result of a higher concentration of clay and thus higher amount of Al replacements in Fe-oxides.

Theoretically, cementing by Fe-oxides can increase aggregate size by connecting more subunits (Totsche et al., 2018) or decrease its size by ‘packing’ the structure resulting in a contraction of the porous structure of colloids, forming a more compact structure also in the low µm scale (Jiang et al., 2014; Jiang et al., 2015). The observed results (increase in size upon Fe oxide removal) support the latter mechanism. The shift in reaggregation sizes to larger diameters after removal of Fe (hydr)oxides (Fig. 5) supports the latter mechanism. Jiang et al. (2015) also observed a size increase of DCB treated fine colloids, probably due to the formation of larger and less stable structures between OC and clay particles. In the present study, such effect likely also occurred for small SMA.

Furthermore, with DCB treatment some nanosized OC was released together with Al and Si (Fig. 6). The detected size range of < 0.02 µm agreed with findings of Kaiser and Guggenberger (2007), who reported that the majority of organic molecules interacting with goethite are in a size range of 0.004-0.01 µm. The

strong linkage of OC with Fe also became evident after reaggregation of DCB treated small SMA, showing that the concentration of nanosized OC was increased.

When targeting to a removal of OC only, the abundance of particles < 1 µm increased at the expense of larger particles (Fig. 3). The released colloids revealed a high Fe, Al, Si, and OC concentration (Fig. 6) that may originate from aluminosilicates or amorphous gibbsite or silica. Colloidal or nano-sized organo/metal oxide/silicate complexes are increasingly recognized as active component of soils (e.g., Tarmat et al., 2019) and their contribution to stable aggregate formation has been suggested (Asano et al., 2018). These colloids remained in suspension even during the reaggregation process (Fig. 5). When OC was present, these colloids were kept within small SMAs. When OC was not present, these colloids were released and did also not reaggregate. To the best of our knowledge this is the first time that it was shown that the OC present in small SMA were physically stabilizing <1 µm colloids and these colloids were not able to re-aggregate by wet/dry cycle without it. The earlier reported role of OC as gluing agent (Abdollahi et al., 2014; Totsche et al., 2018; Wagner et al., 2007) thus applies to both, the general reaggregation capability of small SMA and to the colloid fraction of small SMAs.

5. Conclusions

In this study we showed that the presence of clay and fine colloids promotes the stability of small SMA occlusion in macroaggregates. The presence of Fe and OC, in turn, affect the size distribution and reaggregation capability of small SMA. While Fe cements them so that their size declines, OC mainly glues the colloids within the small SMAs, thus preventing losses of nano-particulate materials during the aggregate formation process. Future research is now needed to spatially resolve the functional involvement of Fe and OC in SMA architecture.

6. Acknowledgements

We acknowledge A. Lindecke for performing the C/N analysis. Furthermore, we want to thank Dr. D. E. Mack and A. Hilgers for supporting the particle size analysis. We also thank P. Narf. This work is associated

to the MAD Soil project (MAD Soil - Microaggregates: Formation and turnover of the structural building blocks of soils), which was funded by the DFG (Deutsche Forschungsgemeinschaft, Research Unit 2179).

7. References

Abdollahi, L., Schjønning, P., Elmholt, S., Munkholm, L.J., 2014. The effects of organic matter application and intensive tillage and traffic on soil structure formation and stability. Soil and Tillage Research 136, 28-37.

Amelung, W., Zech, W., 1999. Minimisation of organic matter disruption during particle-size fractionation of grassland epipedons. Geoderma 92, 73-85.

Asano, M., Wagai, R., 2014. Evidence of aggregate hierarchy at micro- to submicron scales in an allophanic Andisol. Geoderma 216, 62-74.

Asano, M., Wagai, R., Yamaguchi, N., Takeichi, Y., Maeda, M., Suga, H., Takahashi, Y., 2018. In Search of a Binding Agent: Nano-Scale Evidence of Preferential Carbon Associations with Poorly-Crystalline Mineral Phases in Physically-Stable, Clay-Sized Aggregates. Soil Systems. 2, 32.

Barral, M.T., Arias, M., Guérif, J., 1998. Effects of iron and organic matter on the porosity and structural stability of soil aggregates. Soil and Tillage Research 46, 261-272.

Bigham, J.M., Golden, D.C., Buol, S.W., Weed, S.B., Bowen, L.H., 1978. Iron Oxide Mineralogy of Well-drained Ultisols and Oxisols: II. Influence on Color, Surface Area, and Phosphate Retention. Soil Science Society of America Journal 42, 825-830.

Borggaard, O.K., 1988. Phase Identification by Selective Dissolution Techniques, In: Stucki, J.W., Goodman, B.A., Schwertmann, U. (Eds.), Iron in Soils and Clay Minerals. Springer, Dordrecht, Holland, pp. 83-98.

Bronick, C.J., Lal, R., 2005. Soil strcture and management: a review. Geoderma 124, 3–22.

Caravaca, F., Lax, A., Albaladejo, J., 2004. Aggregate stability and carbon characteristics of particle-size fractions in cultivated and forested soils of semiarid Spain. Soil and Tillage Research 78, 83-90.

Chenu, C., Plante, A.F., 2006. Clay-sized organo-mineral complexes in a cultivation chronosequence: revisiting the concept of the 'primary organo-mineral complex'. European Journal of Soil Science 57, 596-607.

Christensen, B.T., 1996. Carbon in primary and secondary organomineral complexes. Advances in Soil Science - Structure and Organic Matter Storage in Agricultural Soils, 97-165.

Christian, P., Von der Kammer, F., Baalousha, M., Hofmann, T., 2008. Nanoparticles: structure, properties, preparation and behaviour in environmental media. Ecotoxicology 17, 326-343.

Churchman, G.J., 2018. Game changer in soil science. Functional role of clay minerals in soil. Journal of Plant Nutrition and Soil Science 181, 99-103.

Darke, A.K., Walbridge, M.R. Estimating non-crystalline and crystalline aluminum and iron by selective dissolution in a riparian forest soil.ommunications in Soil Science and Plant Analysis 25, 11-12.

Denef, K., Six, J., 2005. Clay mineralogy determines the importance of biological versus abiotic processes for macroaggregate formation and stabilization. European Journal of Soil Science 56, 469-479.

Denef, K., Six, J., Bossuyt, H., Frey, S.D., Elliott, E.T., Merckx, R., Paustian, K., 2001. Influence of dry–wet cycles on the interrelationship between aggregate, particulate organic matter, and microbial community dynamics. Soil Biology and Biochemistry 33, 1599-1611.

Duiker, S.W., Rhoton, F.E., Torrent, J., Smeck, N.E., Lal, R., 2003. Iron (Hydr)Oxide Crystallinity Effects on Soil Aggregation. Soil Science Society of America Journal 67, 606-611.

Dultz, S., Woche, S.K., Mikutta, R., Schrapel, M., Guggenberger, G., 2019. Size and charge constraints in microaggregation: Model experiments with mineral particle size fractions. Applied Clay Science 170, 29-40.

Eshel, G., Levy, G.J., Mingelgrin, U., Singer, M.J., 2004. Critical Evaluation of the Use of Laser Diffraction for Particle-Size Distribution Analysis. Soil Science Society of America Journal 68, 736-743.

Eusterhues, K., Rumpel, C., Kögel-Knabner, I., 2005. Organo-mineral associations in sandy acid forest soils: importance of specific surface area, iron oxides and micropores. European Journal of Soil Science 56, 753-763.

Fernández-Ugalde, O., Barré, P., Hubert, F., Virto, I., Girardin, C., Ferrage, E., Caner, L., Chenu, C., 2013. Clay mineralogy differs qualitatively in aggregate-size classes: clay-mineral-based evidence for aggregate hierarchy in temperate soils. European Journal of Soil Science 64, 410-422.
Ferreiro, E.A., Helmy, A.K., De Bussetti, S.G., 1995. Interaction of Fe-oxyhydroxide colloidal particles with montmorillonite. Clay Minerals 30, 195-200.
Fitzpatrick, R.W., Schwertmann, U. 1982. Al-substituted goethite—an indicator of pedogenic and other weathering environments in South Africa. Geoderma 27:335 – 347.
Golchin, A., Oades, J., Skjemstad, J., Clarke, P., 1994. Soil structure and carbon cycling. Soil Research 32, 1043-1068.
Gottselig, N., Nischwitz, V., Meyn, T., Amelung, W., Bol, R., Halle, C., Vereecken, H., Siemens, J., Klumpp, E., 2017. Phosphorus Binding to Nanoparticles and Colloids in Forest Stream Waters. Vadose Zone Journal 16, 1-12.
Guggenberger, G., Kaiser, K., 2003. Dissolved organic matter in soil: challenging the paradigm of sorptive preservation. Geoderma 113, 293-310.
Haynes, R.J., Swift, R.S., 1990. Stability of soil aggregates in relation to organic constituents and soil water content. Journal of Soil Science 41, 73-83.
Jiang, C., Séquaris, J.-M., Wacha, A., Bóta, A., Vereecken, H., Klumpp, E., 2014. Effect of metal oxide on surface area and pore size of water-dispersible colloids from three German silt loam topsoils. Geoderma 235-236, 260-270.
Jiang, X., Bol, R., Nischwitz, V., Siebers, N., Willbold, S., Vereecken, H., Amelung, W., Klumpp, E., 2015. Phosphorus Containing Water Dispersible Nanoparticles in Arable Soil. Journal of Environmental Quality 44, 1772-1781.
Kaiser, K., Guggenberger, G., 2007. Sorptive stabilization of organic matter by microporous goethite: sorption into small pores vs. surface complexation. European Journal of Soil Science 58, 45-59.
Kaiser, M., Berhe, A.A., Sommer, M., Kleber, M., 2012. Application of ultrasound to disperse soil aggregates of high mechanical stability. Journal of Plant Nutrition and Soil Science 175, 521-526.
Kaiser, M., Kleber, M., Berhe, A.A., 2015. How air-drying and rewetting modify soil organic matter characteristics: An assessment to improve data interpretation and inference. Soil Biology and Biochemistry 80, 324-340.
Kiem, R., Kögel-Knabner, I., 2002. Refractory organic carbon in particle-size fractions of arable soils II: organic carbon in relation to mineral surface area and iron oxides in fractions <6 µm. Organic Geochemistry 33, 1699-1713.
Krause, L., Rodionov, A., Schweizer, S.A., Siebers, N., Lehndorff, E., Klumpp, E., Amelung, W., 2018. Microaggregate stability and storage of organic carbon is affected by clay content in arable Luvisols. Soil and Tillage Research 182, 123-129.
Kretzschmar, R. (2005): Soil Colloids and Colloid-Facilitated Transport, in Hillel, D. (ed.): Encyclopedia of Soils in the Environment. Academic Press, New York, NY, USA, pp. 276–284.
Ladd, J.N., Foster, R.C., Skjemstad, J.O., 1993. Soil structure: carbon and nitrogen metabolism. Geoderma 56, 401-434.
Lehmann, J., Kinyangi, J., Solomon, D., 2007. Organic matter stabilization in soil microaggregates: implications from spatial heterogeneity of organic carbon contents and carbon forms. Biogeochemistry 85, 45-57.
Lehtinen, T., Lair, G.J., Mentler, A., Gísladóttir, G., Ragnarsdóttir, K.V., Blum, W.E.H., 2014. Soil Aggregate Stability in Different Soil Orders Quantified by Low Dispersive Ultrasonic Energy Levels. Soil Science Society of America Journal 78, 713-723.
Mehra, O.P., Jackson, M.L., 1958. Iron Oxide Removal from Soils and Clays by a Dithionite-Citrate System Buffered with Sodium Bicarbonate. Clays and Clay Minerals 7, 317-327.
Mikutta, R., Kleber, M., Kaiser, K., Jahn, R., 2005. Organic Matter Removal from Soils using Hydrogen Peroxide, Sodium Hypochlorite, and Disodium Peroxodisulfate. Soil Science Society of America Journal 69, 120-135.
Missong, A., Bol, R., Nischwitz, V., Krüger, J., Lang, F., Siemens, J., Klumpp, E., 2018. Phosphorus in water dispersible-colloids of forest soil profiles. Plant and Soil 427, 71-86.
Neubauer, E., Schenkeveld, W.D.C., Plathe, K.L., Rentenberger, C., von der Kammer, F., Kraemer, S.M., Hofmann, T., 2013. The influence of pH on iron speciation in podzol extracts: Iron complexes with natural organic matter, and iron mineral nanoparticles. Science of The Total Environment 461-462, 108-116.
Oades, J., Waters, A., 1991. Aggregate hierarchy in soils. Soil Research 29, 815-828.

525 Regelink, I.C., Voegelin, A., Koopmans, G.F., Comans, R.N.J. 2014. Characterization of colloidal Fe from
526 soils using field-flow fractionation and Fe K-edge X-ray absorption spectroscopy. Environmental Science
527 and Technology. 48, 4307-4316.
528 Schwertmann, U., Carlson, L. (2005). The pH-dependent transformation of schwertmannite to goethite at
529 25 °C. Clay Minerals. 40, 63-66.
530 Siebers, N., Abdelrahman, H., Krause, L., Amelung, W., 2018a. Bias in aggregate geometry and properties
531 after disintegration and drying procedures. Geoderma 313, 163-171.
532 Siebers, N., Bauke, S.L., Tamburini, F., Amelung, W. 2018b. Short-term impacts of forest clear-cut on P
533 accessibility in soil microaggregates: An oxygen isotope study. Geoderma 315, 59-64.
534 Siebers, N., Kruse, J. 2019. Short-term impacts of forest clear-cut on soil structure and consequences for
535 organic matter composition and nutrient speciation: A case study. PLoS ONE 14, e0220476.
536 Six, J., Bossuyt, H., Degryze, S., Denef, K., 2004. A history of research on the link between
537 (micro)aggregates, soil biota, and soil organic matter dynamics. Soil and Tillage Research 79, 7-31.
538 Six, J., Conant, R.T., Paul, E.A., Paustian, K., 2002. Stabilization mechanisms of soil organic matter:
539 Implications for C-saturation of soils. Plant and Soil 241, 155-176.
540 Snyder, V.A., Vázquez, M.A., 2005. STRUCTURE, In: Hillel, D. (Ed.), Encyclopedia of Soils in the
541 Environment. Elsevier, Oxford, pp. 54-68.
542 Sowers, T.D., Stuckey, J.W., Sparks, D.L., 2018. The synergistic effect of calcium on organic carbon
543 sequestration to ferrihydrite. Geochemical Transactions 19, 4.
544 Tamrat, W.Z.; Rose, J.; Grauby, O.; Doelsch, E.; Levard, C.; Chaurand, P.; Basile-Doelsch, I. Soil-organo
545 mineral associations formed by co-precipitation of Fe, Si and Al in presence of organic ligands.
546 Geochimica et Cosmochimica Acta 260: 15-28.
547 Tan, T. S., Phoon, K. K., Hight, D. W., and Leroueil, S. (2006). “Characterisation and Engineering Properties
548 of Natural Soils,” in Proceedings of the Second International Workshop on Characterisation and
549 Engineering Properties of Natural Soils (Boca Raton: CRC Press).
550 Tisdall, J.M., 1996. Formation of soil aggregates and accumulation of soil organic matter, In: Carter, M.R.,
551 Stewart, B.A. (Eds.), Structure and organic matter storage in agricultural soils. Taylor & Francis, Boca
552 Raton, USA, pp. 57-87.
553 Tisdall, J.M., Oades, J.M., 1982. Organic matter and water-stable aggregates in soils. Journal of Soil
554 Science 33, 141-163.
555 Totsche, K.U., Amelung, W., Gerzabek, M.H., Guggenberger, G., Klumpp, E., Knief, C., Lehndorff, E.,
556 Mikutta, R., Peth, S., Prechtel, A., Ray, N., Kögel-Knabner, I., 2018. Microaggregates in soils. Journal of
557 Plant Nutrition and Soil Science 181, 104-136.
558 Utomo, W.H., Dexter, A.R., 1982. Changes in soil aggregate water stability induced by wetting and drying
559 cycles in non-saturated soil. Journal of Soil Science 33, 623-637.
560 Varadachari, C., Goswami, G., Ghosh, K., 2006. Dissolution of Iron Oxides. Clay Research 25, 1-22.
561 Virto, I., Barré, P., Chenu, C., 2008. Microaggregation and organic matter storage at the silt-size scale.
562 Geoderma 146, 326-335.
563 Wagai, R., Mayer, L.M., 2007. Sorptive stabilization of organic matter in soils by hydrous iron oxides.
564 Geochimica et Cosmochimica Acta 71, 25-35.
565 Wagner, S., Cattle, S.R., Scholten, T., 2007. Soil-aggregate formation as influenced by clay content and
566 organic-matter amendment. Journal of Plant Nutrition and Soil Science 170, 173-180.
567 Weil, R.R., Brady, N.C., 2017. The Nature and Properties of Soils, 15 ed. Pearson Education Limited,
568 Harlow, England.
569 Zhao, Q., Poulson, S.R., Obrist, D., Sumaila, S., Dynes, J.J., McBeth, J.M., Yang, Y., 2016. Iron-bound
570 organic carbon in forest soils: quantification and characterization. Biogeosciences 13, 4777-4788.

8. Figure legends

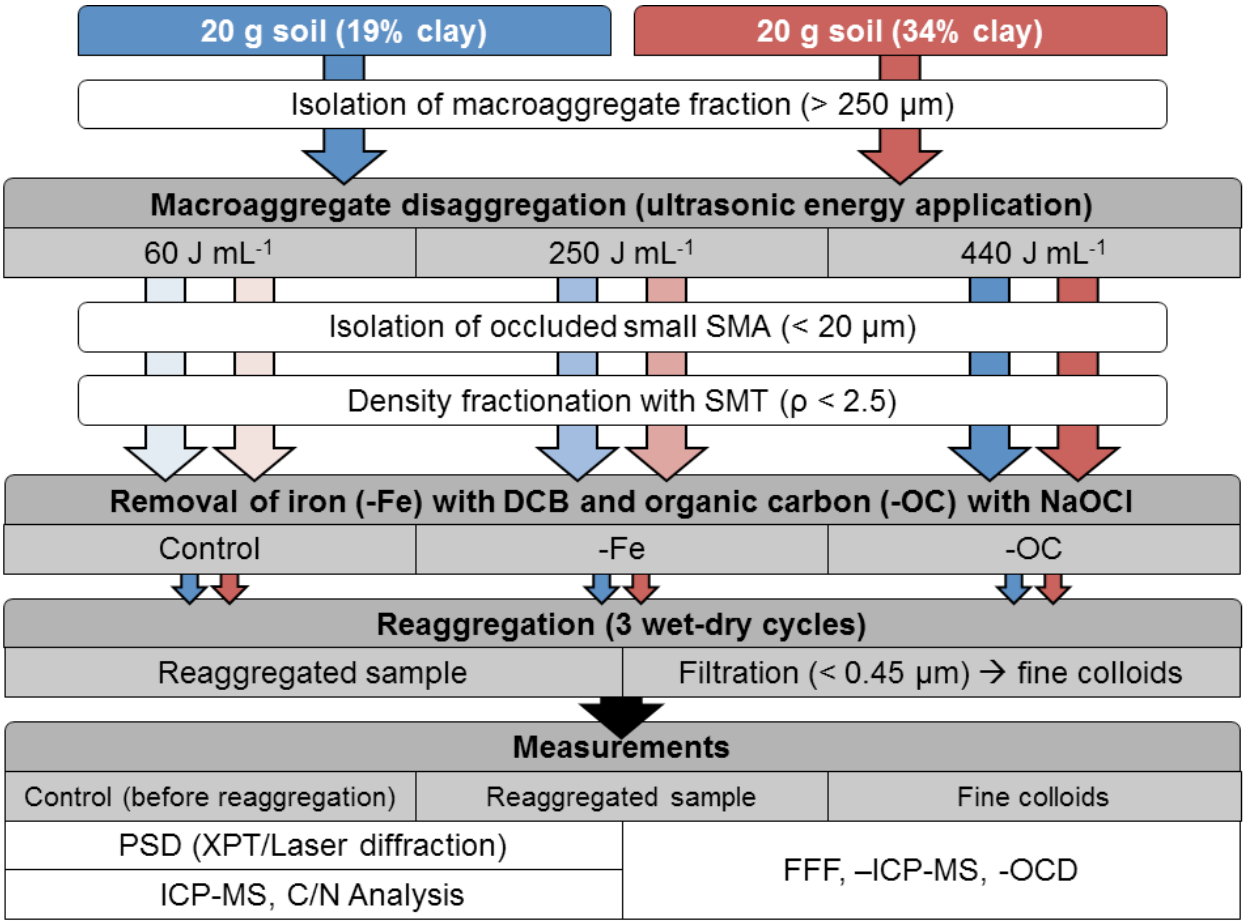

Figure 1: Scheme illustrating the procedure of sample preparation and analysis. Overall three replicates were selected for each soil with small- (19%, blue) and large- (34%, red) clay content. Occluded small soil microaggregates < 20 µm (SMA) were released from macroaggregates using three different levels (three different shaded arrows) of ultrasonic energy. Small SMA were isolated by density fractionation in sodium metatungstate (SMT). Iron was removed (-Fe) using dithionite-citratebicarbonate (DCB) and organic carbon was removed (-OC) using sodium hypochlorite (NaOCl). The reaggregation was performed on small SMA released with the highest ultrasonic level and samples were analyzed for their size distribution (PSD) using a microparticle detector (XPT) and laser diffraction. Fine colloids were fractionated with field-flow fractionation (FFF) and their elemental composition was analyzed online using inductively coupled plasma mass spectrometry (ICP-MS) and an organic carbon detector (OCD).

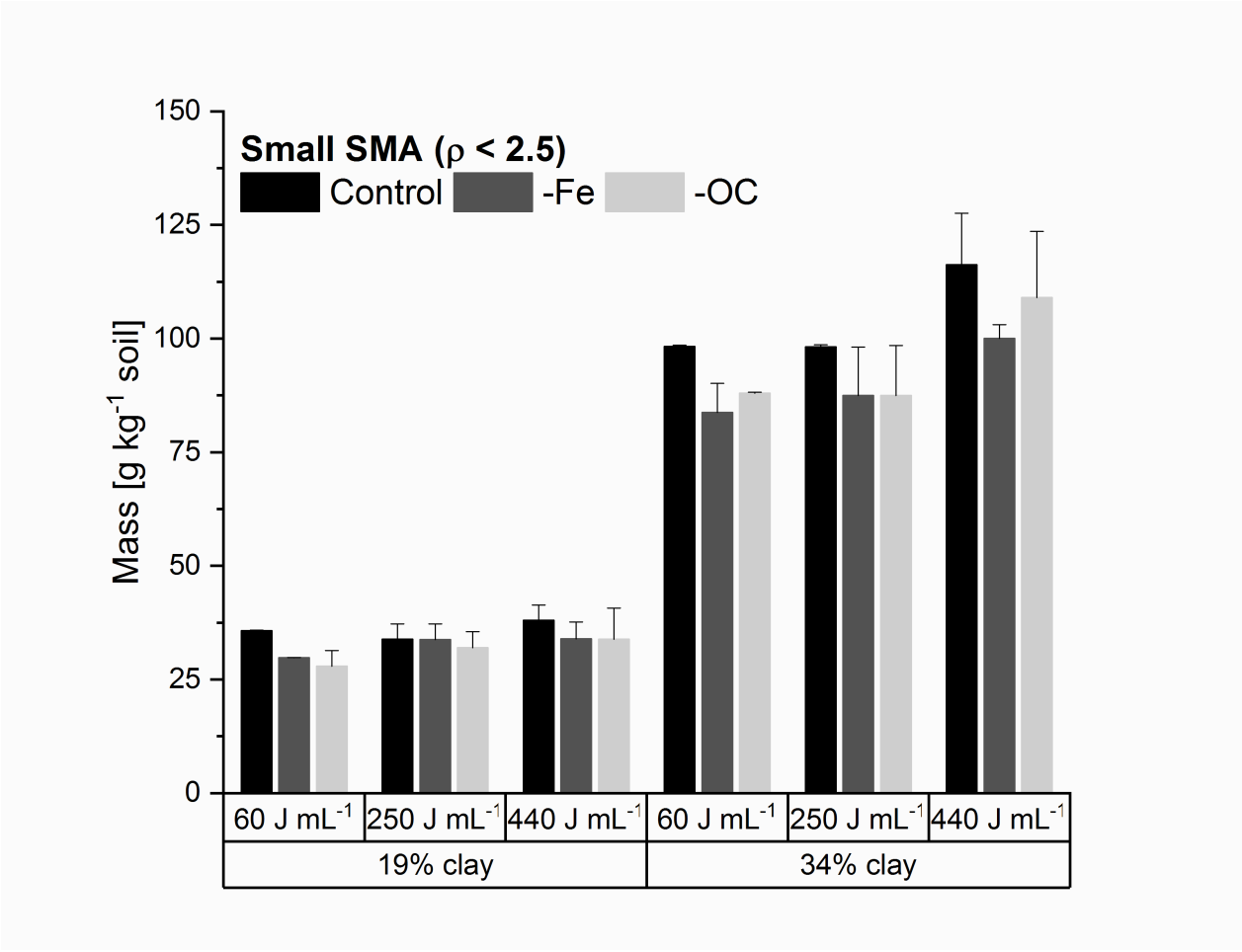

585

586 **Figure 2:** Mass of the small soil microaggregate < 20 µm (SMA) fraction released from macroaggregates
587 with three levels of ultrasonic energy (60, 250, and 440 J mL^{-1}). Masses are shown for the control (black),
588 and after the reduction of iron with dithionite-citratebicarbonate (DCB) (-Fe, grey) and organic carbon with
589 NaOCl (-OC, light grey). Error bars represent standard deviation (SD).

590

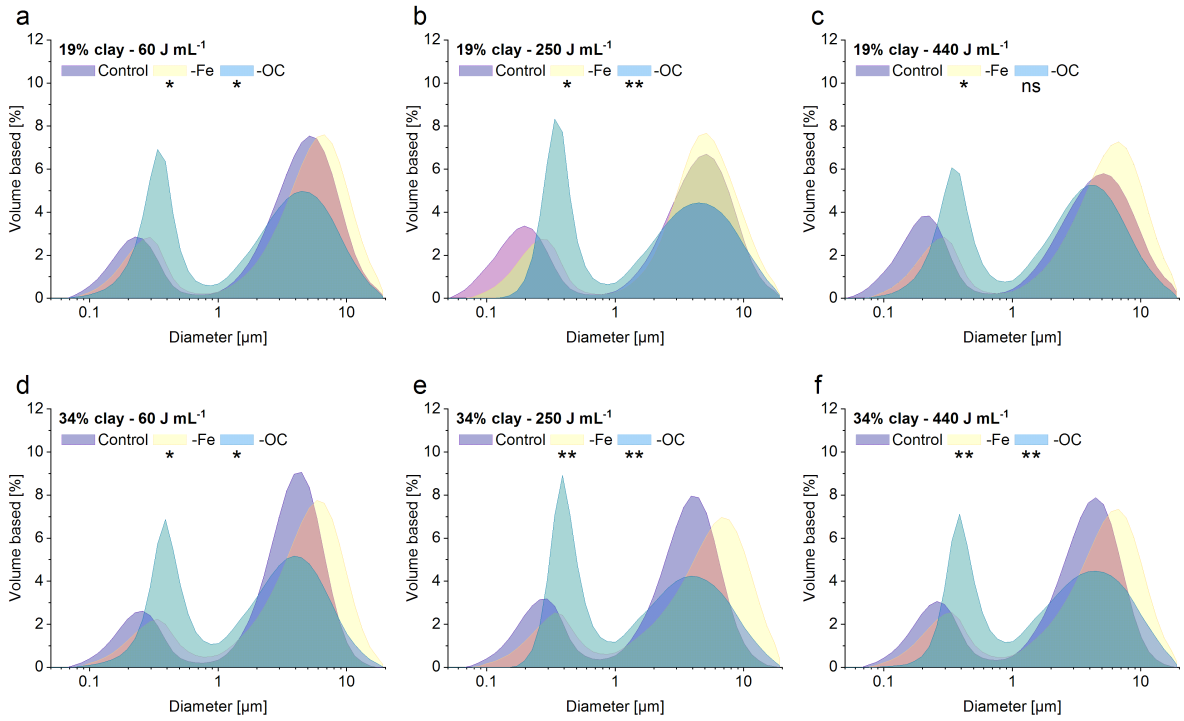

591

592 **Figure 3:** Volume based size distribution of the small soil microaggregate < 20 µm (SMA) fraction before
593 aggregation measured by laser diffraction. The size distributions are shown for the soils with small (19%, **a-**
594 **c**) and large (34%, **d-f**) clay content, from which occluded small SMA were isolated with different ultrasonic
595 energies (60 (**a+d**), 250 (**b+e**) and 440 (**c+f**) J mL^{-1}) and chemically treated (Control (purple), reduction of
596 iron (-Fe, yellow), reduction of organic carbon (-OC, blue)). Significant differences to control are indicated
597 in asterisks.

598

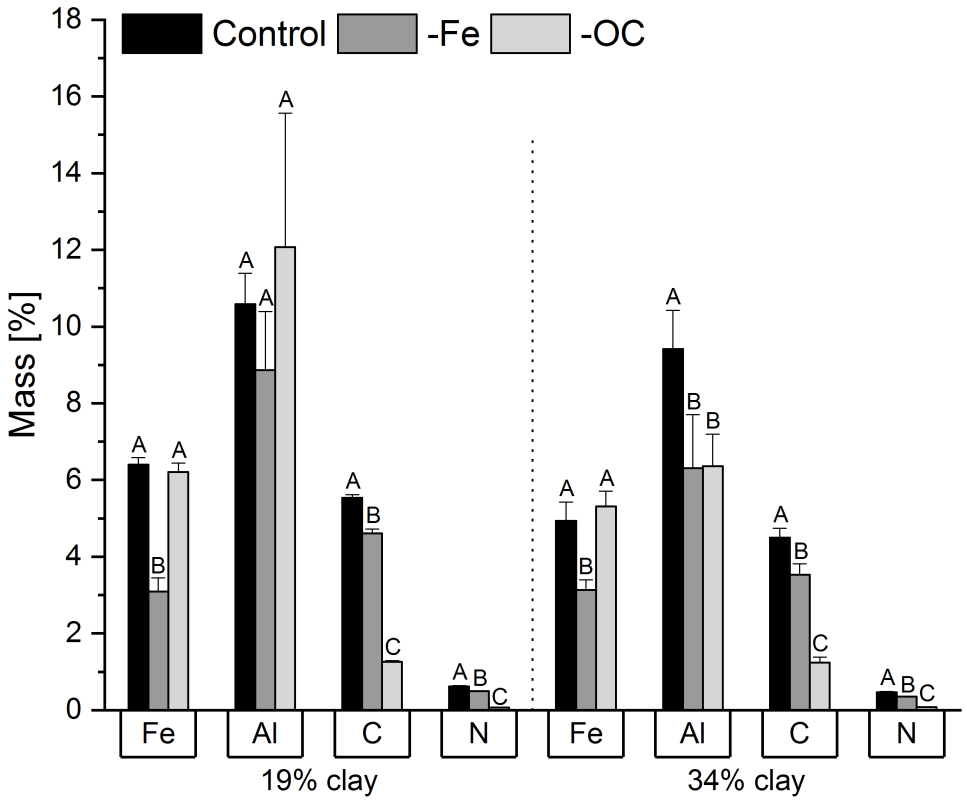

599

600 **Figure 4:** Average abundance of elements as weight percentage of small soil microaggregates < 20 µm
601 (SMA) for the control group (black) and treatments with dithionite-citratebicarbonate (DCB) (- Fe, grey) and
602 NaOCl (-OC, light grey). Significant differences between the treatments are indicated with different capital
603 letters. Error bars represent standard deviation (SD).

604

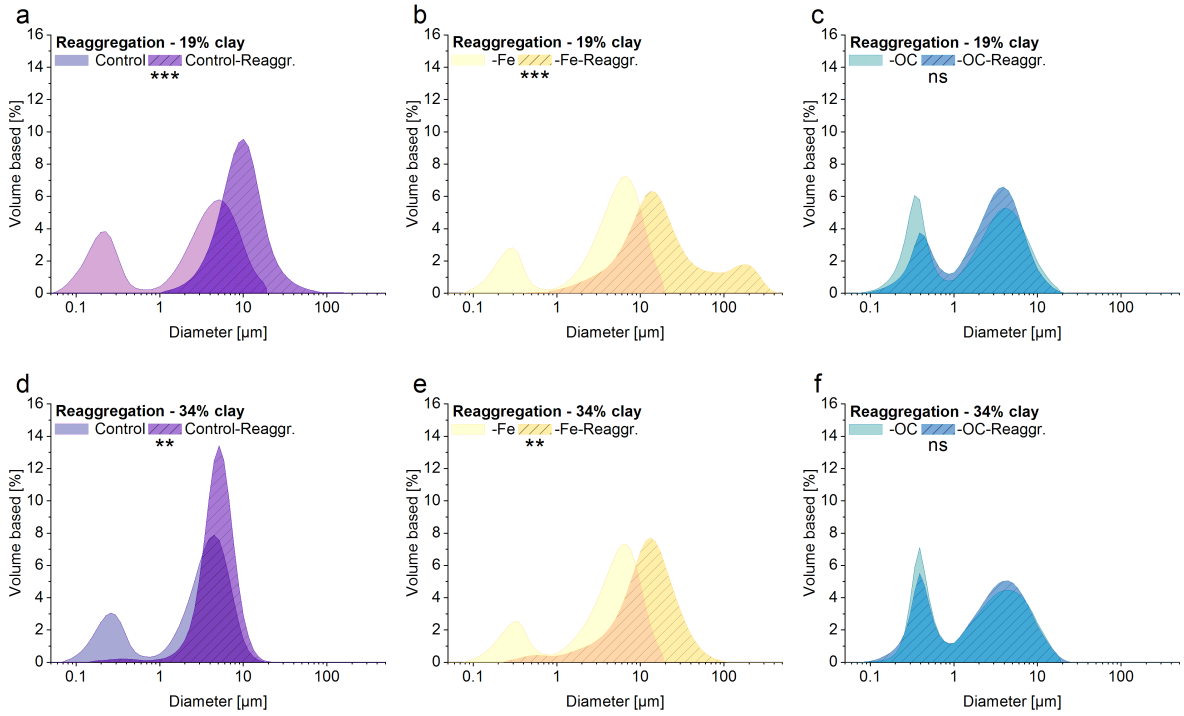

605

606 **Figure 5:** Volume based size distribution of the small soil microaggregate < 20 µm (SMA) fraction after
607 reaggregation measured by laser diffraction. The size distributions are shown for the soils with small (19%,
608 **a-c**) and large (34%, **d-f**) clay content and different chemical pre-treatments (Control (purple), reduction of
609 iron (-Fe, yellow), reduction of organic carbon (-OC, blue)). Significant differences to the size distribution
610 before reaggregation are indicated in asterisks.

611

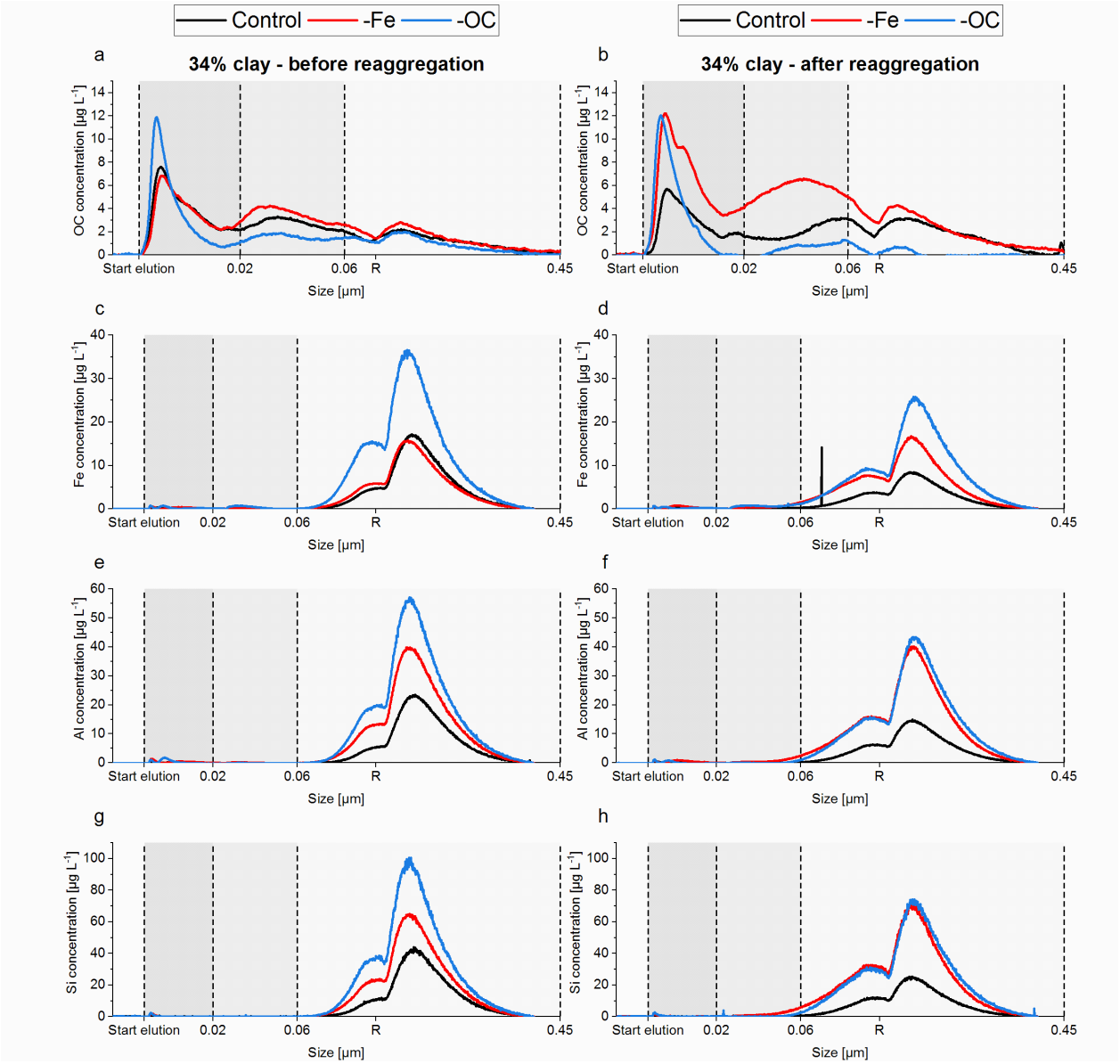

612

613 **Figure 6:** Fractograms of fine colloid fractions < 0.45 µm from soils with large clay content (34%) analyzed
614 by FFF-OCD-ICP-MS before (left side, **a,c,e,g**) and after (right side, **b,d,f,h**) reaggregation. The top row
615 (**a,b**) shows the signal measured by the organic carbon detector (OCD). According the elution time different
616 size classes were defined (0.02, 0.06, and 0.45 µm). With inductively coupled plasma mass spectrometry
617 (ICP-MS), the chemical composition of fine colloids was analyzed showing the concentration of iron (Fe,
618 **c,d**), aluminum (Al, **e,f**), and silicon (Si, **g,h**) during elution. Different pre-treatments are indicated in different
619 colors including control (black), reduction of Fe (-Fe, red), and reduction of organic carbon (-OC, blue). The
620 release-peak is indicated with the letter R.

621

Tables

Table 1. Elemental composition of bulk soil and small soil microaggregates (SMA), n= 3, ± standard deviation (SD).

Table 1: Bulk elements of sampled soils

Clay	19%	34%
Elements [g kg^{-1}]		
Bulk Al_D	1.2 ± 0.0	1.5 ± 0.1
Bulk Fe_D	7.0 ± 0.0	8.5 ± 0.1
Bulk Mn_D	0.5 ± 0.0	1.3 ± 0.0
SMA OC [g kg^{-1}]		
<250 µm (free)	17.5 ± 1.1	31.6 ± 1.0
<250 µm(occluded)	27.5 ± 1.1	30.8 ± 1.3
SMA N [g kg^{-1}]		
<250 µm (free)	1.9 ± 0.1	3.2 ± 0.1
<250 µm(occluded)	3.0 ± 0.1	3.1 ± 0.1
SMA C/N ratio		
<250 µm (free)	9.5 ± 0.3	9.9 ± 0.2
<250 µm(occluded)	9.3 ± 0.1	10.0 ± 0.3

Al_D, Fe_D, and Mn_D : Dithionite-Citrate-Bicarbonate (DCB) extractable Al, Fe, and Mn concentrations.

Appendix Figure legend

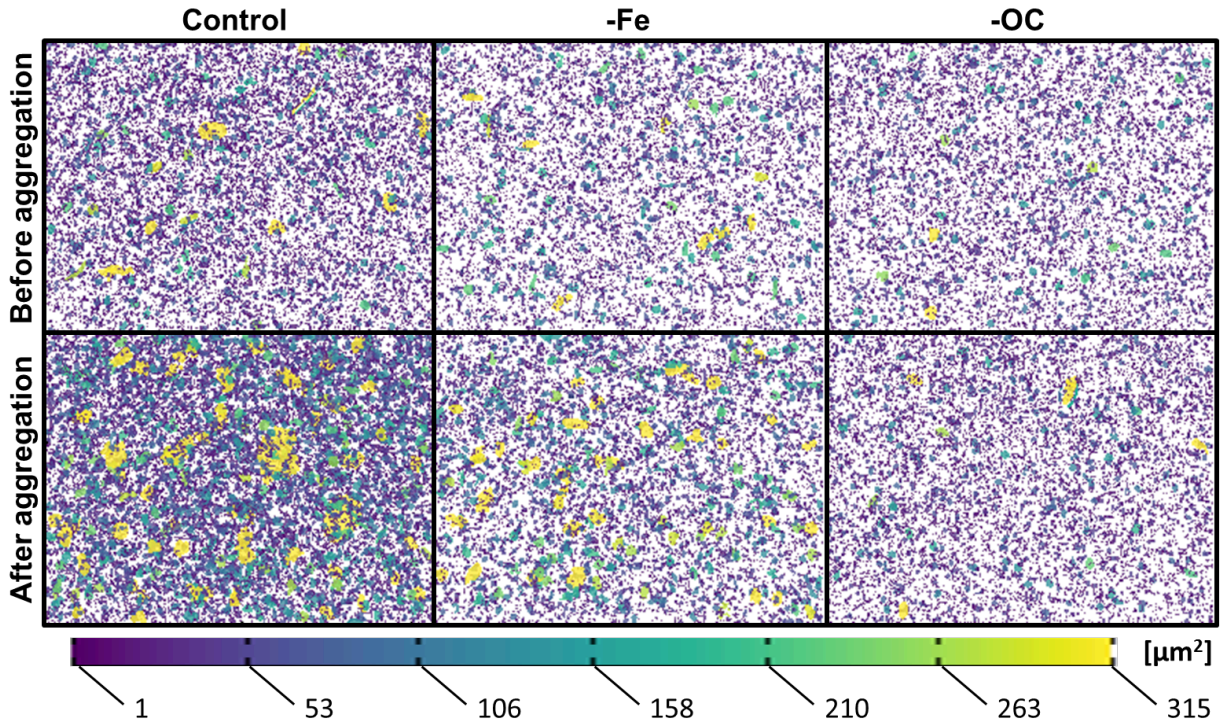

629

630 Figure A.1: Exemplary overlays of micrographs measured by a microparticle detector (XPT) showing the measured
631 suspensions of small soil microaggregates < 20 µm (SMA) before (top row) and after the aggregation (bottom row)
632 with control samples (left) and after the reduction of iron (-Fe, middle) and organic carbon (-OC, right). Different sized
633 areas of each individual particle/aggregate are indicated in different colors (see scale bar).

634

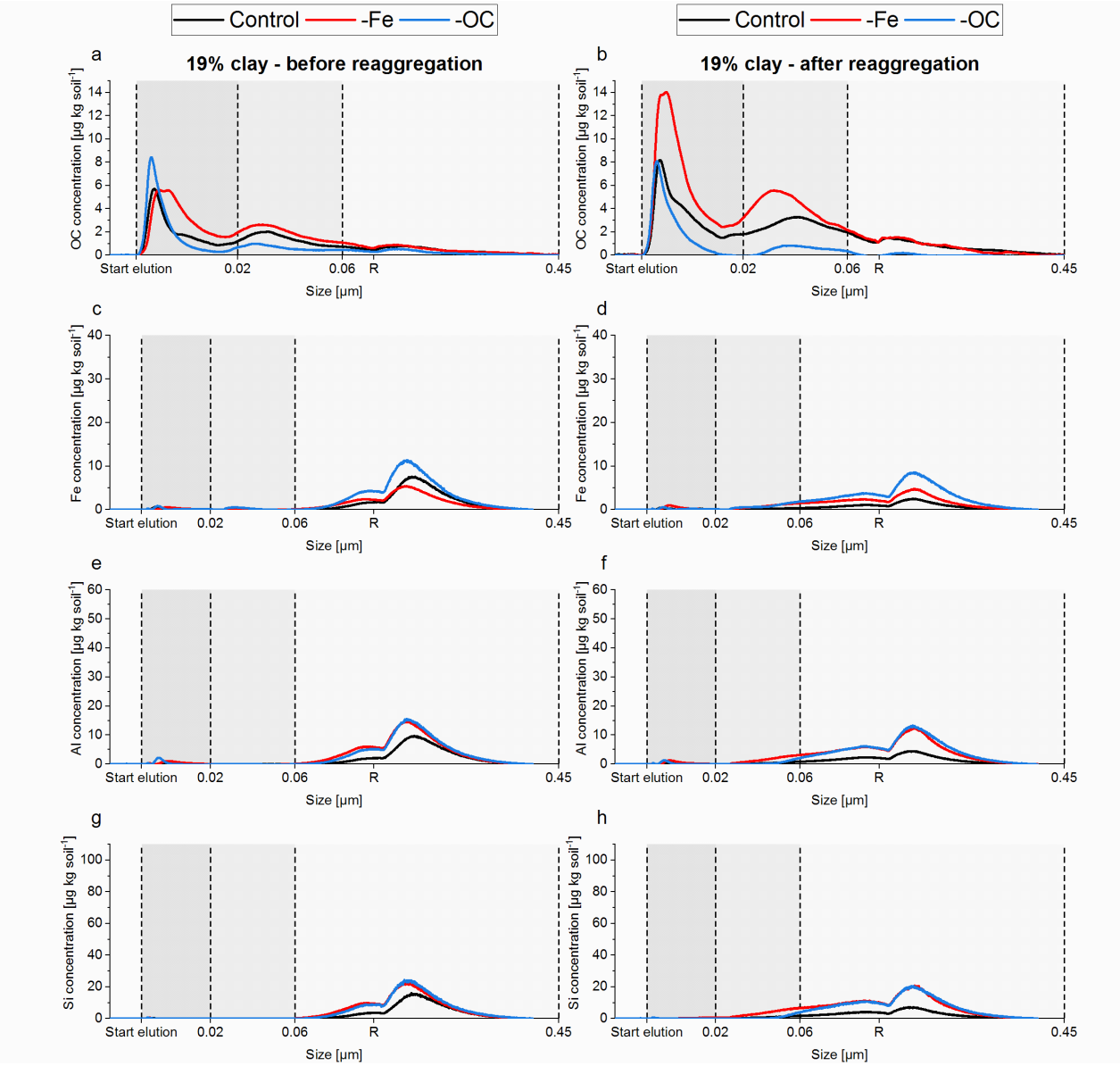

Figure A.2: Fractograms of fine colloid fractions < 0.45 µm from soils with small clay content (19%) analyzed by FFF-OCD-ICP-MS before (left side, a,c,e,g) and after (right side, b,d,f,h) reaggregation. The top row (a,b) shows the signal measured by the organic carbon detector (OCD). According the elution time different size classes were defined (0.02, 0.06, and 0.45 µm). With inductively coupled plasma mass spectrometry (ICP-MS), the chemical composition of fine colloids was analyzed showing the concentration of iron (Fe, c,d), aluminum (Al, e,f), and silicon (Si, g,h) during elution. Different pre-treatments are indicated in different colors including control (black), reduction of Fe (-Fe, red), and reduction of organic carbon (-OC, blue). The release-peak is indicated with the letter R.

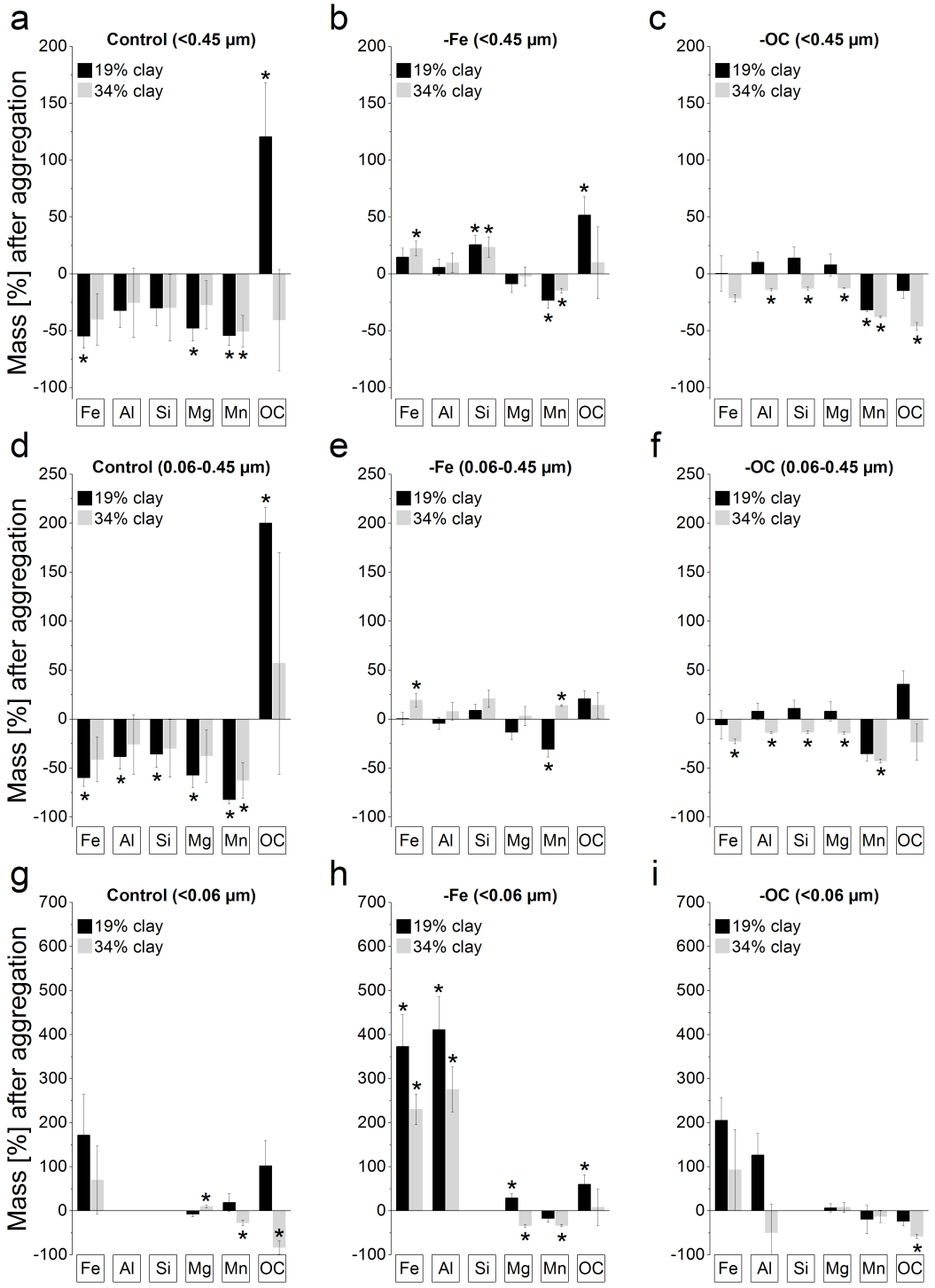

644

645 Figure A.3: Mass-change of elements iron (Fe), aluminum (Al), silicon (Si), magnesium (Mg), manganese (Mn), and
646 organic carbon (OC) after reaggregation in fine colloids (< 0.45 µm, a-c), and in the size range of 0.45-0.06 µm (d-f)
647 and < 0.06 µm (g-i) isolated from soils with small (19%, black) and large (34%, grey) clay content.